Supporting Information:

Figure S1. Plasmid copy number effects P*emrR*-GFP biosensor activation. Compound dependent activation of the P*emrR*-GFP biosensor was assessed after 2 hrs under single copy (BLUE) and high-copy (PINK) number for concentrations of 0.25 and 1mM. Error bars represent 95% confidence intervals (n=3).

Figure S2. Screening environmental isolates with the P*emrR*-GFP biosensor. Soil isolates, including known lignin degraders *R. jostii* RHA1 and *E. lignolyticus* SCF1, were cultured in the presence of HP-L™ for 2 weeks with (PINK) and without (BLUE) a solid phase of 0.4% agarose. Culture supernatant was then added to a P*emrR*-GFP biosensor culture and incubated for 2 hrs before measuring fluorescence. Error bars represent 95% confidence intervals (n=3).

Figure S3. (A) *emrRAB* promoter activation in *emrR* and *emrB* knockout backgrounds. Time course GFP fluorescence measurements for 1 mM of vanillin (PINK), vanillic acid (BLUE), and vanillyl alcohol (BLACK) in wild-type, emrR and emrB knockout backgrounds (n=3). (B) Growth kinetics of *emrR* and *emrB* knockouts using sub-inhibitory concentrations of monoaromatic compounds. Wild-type (BLACK), *emrR* (-) (PINK), and *emrB*(-) (BLACK) strains were grown in the presence of 0.5 mM of various monoaromatic compounds (n=3**).**

Figure S4. (A) Effect of *emrR* knockout on growth kinetics in the presence of enzyme treated lignin. The effect of 0.5 g/L of SF-HKL (PINK) and DypB N246A treated SF-HKL (BLUE) in *emrR* and *emrB* knockout backgrounds (n=3). (B) EmrR overexpression improves growth kinetics of *E. coli* exposed to inhibitory levels of monoaromatic compounds. Growth kinetics with uninduced (BLUE) and induced (PINK) expression of EmrR from high-copy plasmid pBAD24. Error bars represent 95% confidence intervals (n=3).

Figure S5. (A) Taxonomic distribution of fosmid end sequences. Fosmid end sequences were phylogenetically assigned using SOrt-ITEMS for CO182 (12,630 sequences) and CO182 (12,599 sequences). (B) Fosmid library screening by co-culture with the P*emrR*-GFP biosensor for 8 x 384-well plates with selected hits (PINK). (C) Validation of select fosmid clones by repeat screening. Error bars represent 95% confidence intervals (n=3).

Figure S6. Precipitation phenotypes. Various fosmid clones incubated alone or in combination with SF-HKL or HP-L™ in minimal media for 16 hrs.

Figure S7. Genetic context maps for active fosmids. Functional classes related to lignin degradation, CAZy auxiliary enzymes, mobile elements, transposon insertions, and tRNAs are annotated. Transposon insertions that caused a statistically significant decrease in GFP signal were identified using a Z-score ratio. The G+C ratio for every 200 nucleotides and gene abundance determined by mapping over 500 million Illumina HiSeq reads sourced from the coal bed milieu is also displayed. Connections represent protein homologs with minimum 50% identity and an e-value of 10E-20. Due to size limitations, a gap was inserted in fosmid CO182_08_C21 and the complete fosmid structure is represented in Figure S10.

Figure S8. (A) GC-MS of SF-HKL incubated with the clone 182_08_C21 (BLUE) and its transposon mutants at the position 4949 (black) and 55060 (BLACK). Insertion mutants reducing or abolishing lignin transformation, including insertions in *copA*, were identified by screening with the P*emrR*-GFP biosensor. The data was normalized to an empty fosmid clone. Products identified using a catalogue search included 2,4-dihydroxybenzoic acid (t_r 12.4), 1,4-dihydroxy-2,6-dimethoxybenzene (t_r 13.5) and benzoic acid(t_r 15.7) (n = 2). (B) Structure based sequence alignment of CopA generated using 3D-Coffee. The structures of MCOs from six different organisms: *Homo sapiens* (PDB ID: 1KCW), *Streptomyces viridosporus* T7A (PDB ID: 3TAS), a marine metagenome (PDB ID: 4F7K), and *Thermus thermophilus* (PDB ID: 2XU9) were selected from the protein data bank. The resulting alignment was edited manually to show the structurally conserved regions. The copper binding motifs (HxHx, HxH, HxxHxH and

HCHxxxHxxxxM/L/F) are highlighted in the red box. (C) SDS-PAGE of CopA. Lane 1, protein molecular weight marker; lane 2, total protein; lane 3, soluble portion; lane 4, eluate from Ni-NTA column. (D and E) CopA-catalyzed oxidation of 2,6-DMP. Reaction mixtures contained 1 mM 2,6-DMP, 1% DMSO and either 30 nM CopA and 5 mM $CuSO_4$ or 200 nM CopA (E) (20 mM sodium phosphate, pH 8, 25 °C). No enzyme controls are shown in black.

Figure S9. Comparative gene content analysis of active fosmid clones conferring lignin transformation phenotypes. Histogram depicting annotated genes within the six functional classes implicated in (A) lignin transformation phenotypes (out of 813 total genes) or (B) mobile genetic elements. Circos representations showing nucleotide and protein level homology using all-against-all blastn (RED connections, E-value cutoff 10E-5) and tblastn (BLUE connections, E-value cutoff 10E-50), respectively.

Figure S10. The gene content of several active fosmid clones maps to the flexible genomes of sequenced reference strains. The percent identity of reciprocal best blast hits (RBHs) between *Pseudomonas strutzeri* A1501 and *P. strutzeri* ATCC 17588 is plotted with respect to their location in the A1501 genome to identify the core and non-shared regions. Red vertical bars indicate regions where three or more consecutive fosmid genes map to the A1501 genome with greater than 60% protein identity. Green ORFs represent fosmid derived sequences, blue ORFs represent related *P. strutzeri* A1501 sequences, and grey connections between genes indicates percent identity between proteins greater than 60%.

Figure S11. A conceptual model for bacterial lignin transformation based on horizontal gene transfer and gene shuffling. Related organisms generate different monoaromatic lignin transformation products based on the arrangement, repeat structure and diversity of the 6 functional classes identified in this study. HGT events can augment or reprogram functional arrays giving rise to synergistic capabilities reflected in a new monaromatic transformation profile. In step 1, protein secretion machinery allows for the export of both lignin transforming enzymes and those generating reactive oxygen species such as

hydrogen peroxide. Monoaromatic products are alleviated from the lignin polymer and enter or leave the cell via small molecule transporters, which often fall within the multidrug efflux superfamily (Step 2). Signal transducers (with PAS domains) recognize different components of lignin structure (or resulting redox state) (Step 3) and integrate this information (along with breakdown products) to modulate expression via a transcription factor (such as an EmrR homolog)(Step 4). Finally, Step 5 shows how chemotaxis can also be affected through MCPs to bias movement towards or away from the lignin structure or products to maximize enzyme activity while protecting the cell from free radical damage.

Table S1. Quantification of select compounds in mg L^{-1} calculated from standard curves on GC-MS.

Table S2. Summary of fosmid annotations, evidence of secretion and class assignments. Domains are also annotated to support functional class assignment.

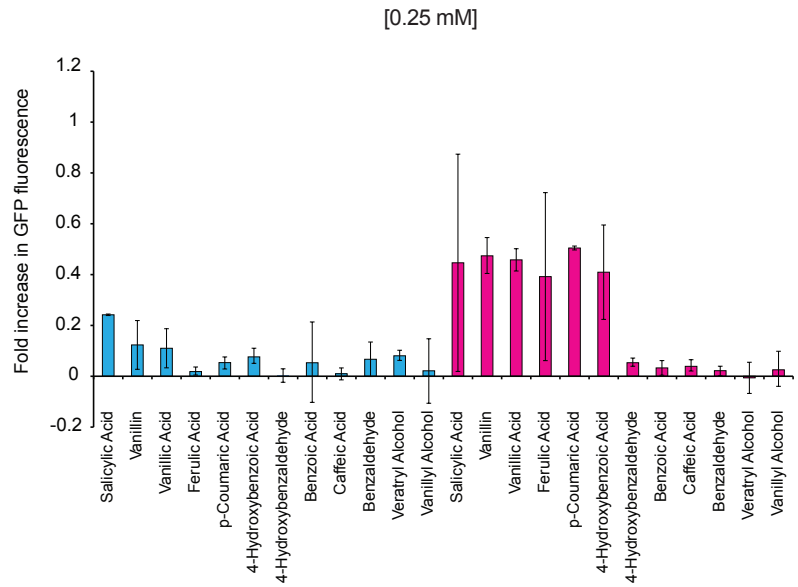
[0.25 mM]
Fold increase in GFP fluorescence
1.2
1
0.8
0.6
0.4
0.2
0
-0.2
Salicylic Acid
Vanillin
Vanilic Acid
Ferulic Acid
p-Coumaric Acid
4-Hydroxybenzoic Acid
4-Hydroxybenzaldehyde
Benzoic Acid
Caffeic Acid
Benzaldehyde
Veratryl Alcohol
Vanillyl Alcohol
Salicylic Acid
Vanillin
Vanilic Acid
Ferulic Acid
p-Coumaric Acid
4-Hydroxybenzoic Acid
4-Hydroxybenzaldehyde
Benzoic Acid
Caffeic Acid
Benzaldehyde
Veratryl Alcohol
Vanillyl Alcohol

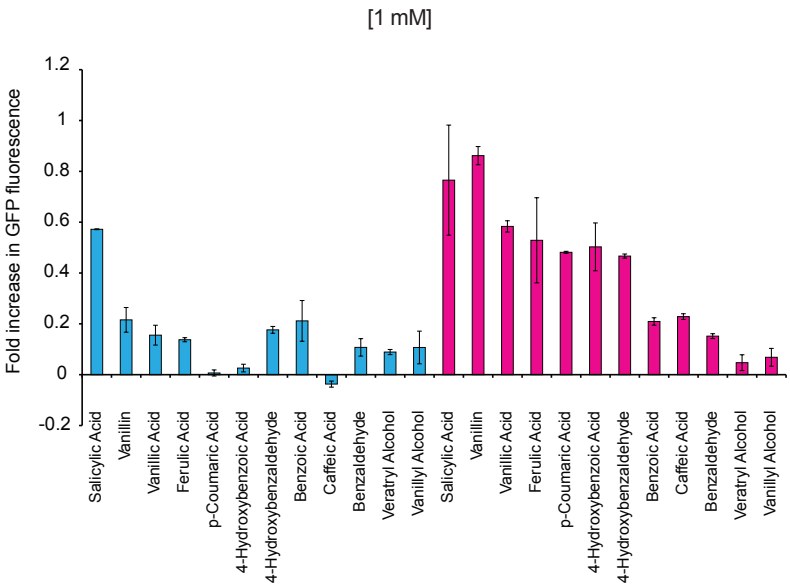
[1 mM]
Fold increase in GFP fluorescence
1.2
1
0.8
0.6
0.4
0.2
0
-0.2
Salicylic Acid
Vanillin
Vanilic Acid
Ferulic Acid
p-Coumaric Acid
4-Hydroxybenzoic Acid
4-Hydroxybenzaldehyde
Benzoic Acid
Caffeic Acid
Benzaldehyde
Veratryl Alcohol
Vanillyl Alcohol
Salicylic Acid
Vanillin
Vanilic Acid
Ferulic Acid
p-Coumaric Acid
4-Hydroxybenzoic Acid
4-Hydroxybenzaldehyde
Benzoic Acid
Caffeic Acid
Benzaldehyde
Veratryl Alcohol
Vanillyl Alcohol

Fig. S1

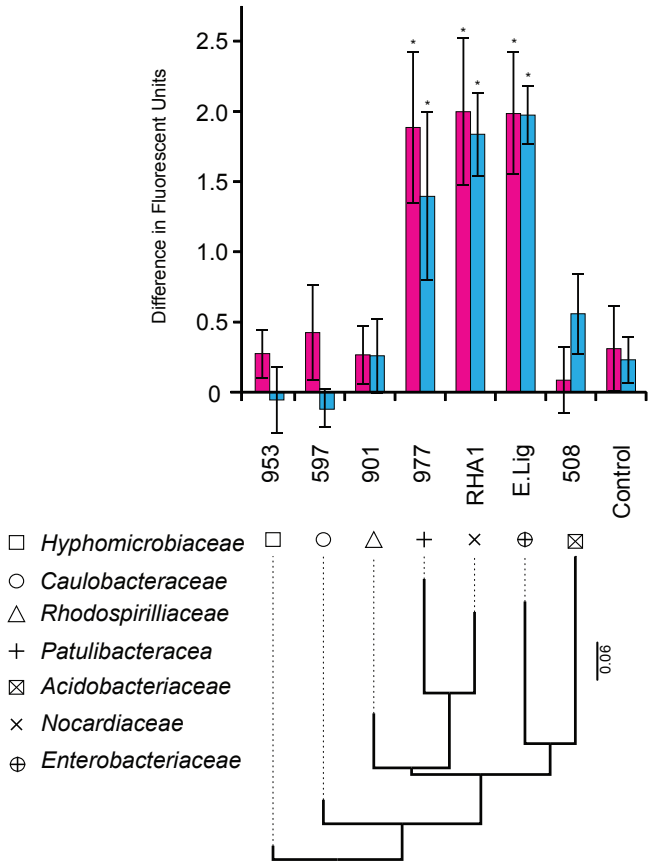
Difference in Fluorescent Units
2.5
2.0
1.5
1.0
0.5
0
953
597
901
977
RHA1
E.Lig
508
Control
□ Hyphomicrobiaceae
○ Caulobacteraceae
△ Rhodospirilliaceae
+ Patulibacteracea
⊠ Acidobacteriaceae
× Nocardiaceae
⊕ Enterobacteriaceae
0.06

Fig. S2

A

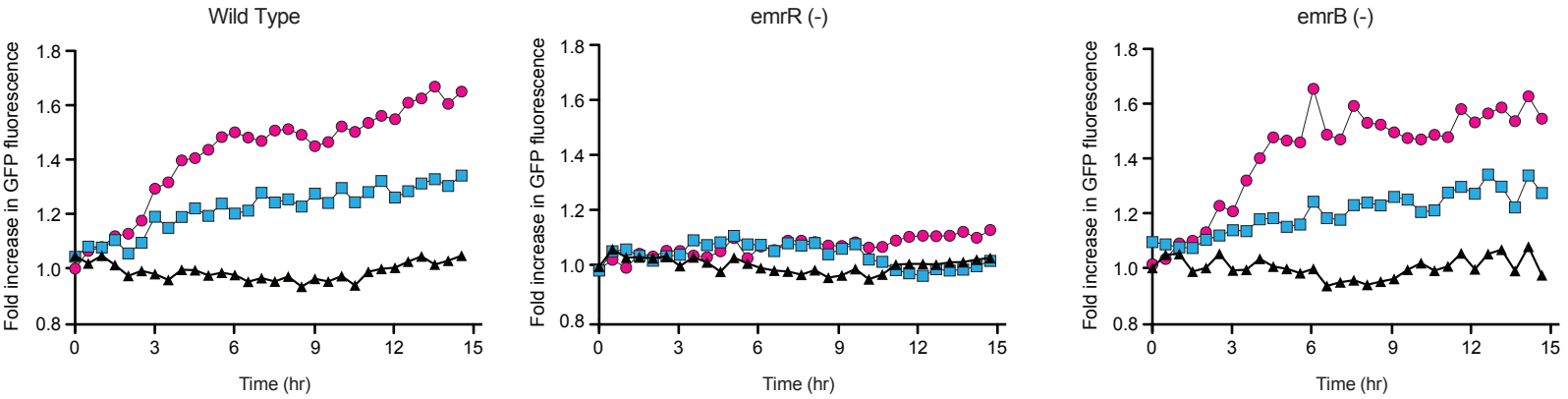
Wild Type
emrR (-)
emrB (-)
Fold increase in GFP fluorescence
Time (hr)

B

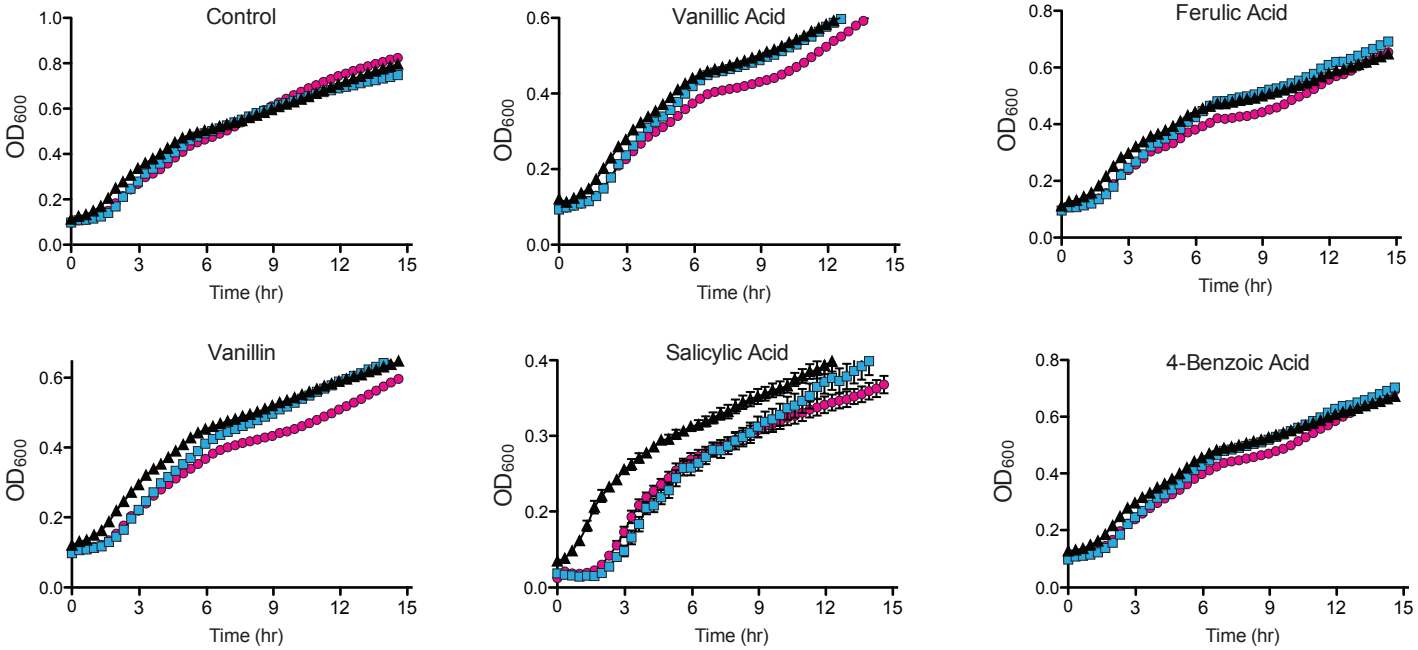
Control
Vanillic Acid
Ferulic Acid
Vanillin
Salicylic Acid
4-Benzoic Acid
OD600
Time (hr)

Fig. S3

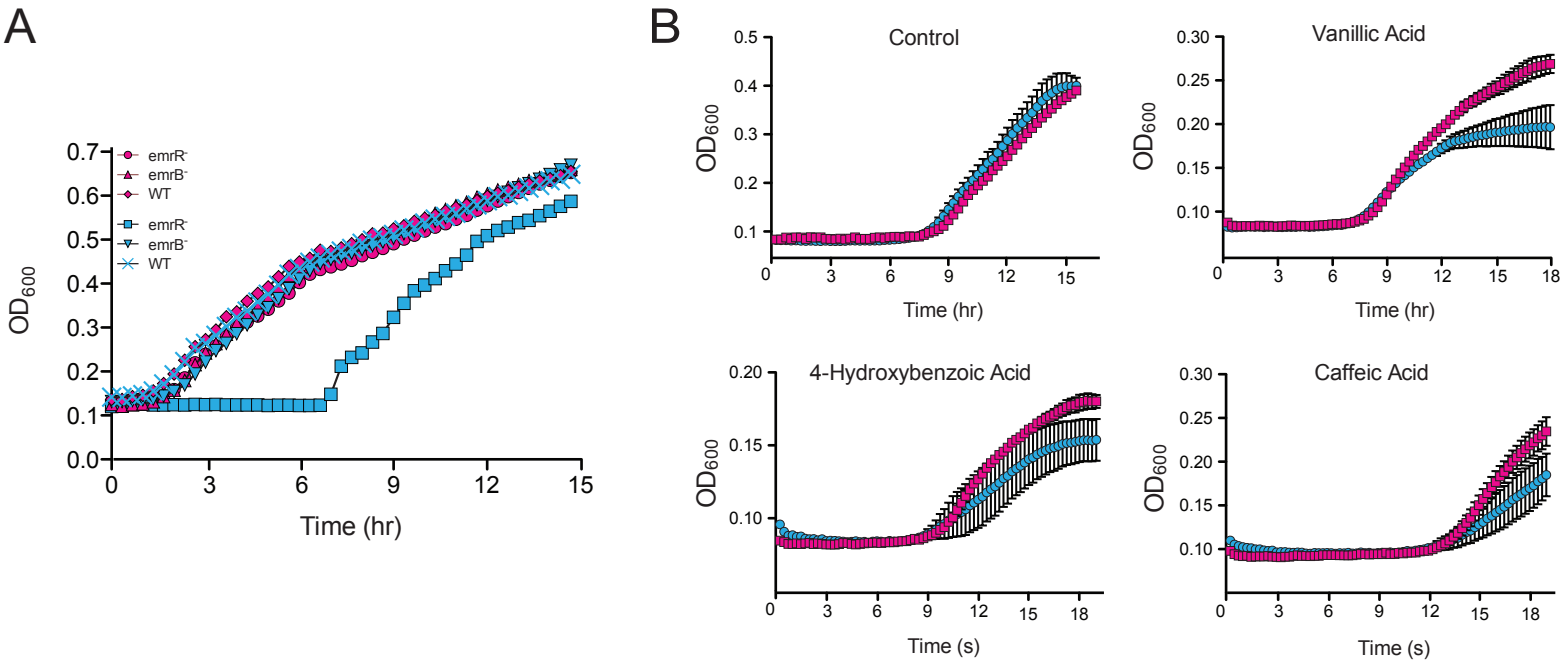
A
B
emrR-
emrB-
WT
OD600
Time (hr)
Control
Vanillic Acid
4-Hydroxybenzoic Acid
Caffeic Acid
Time (s)

Fig. S4

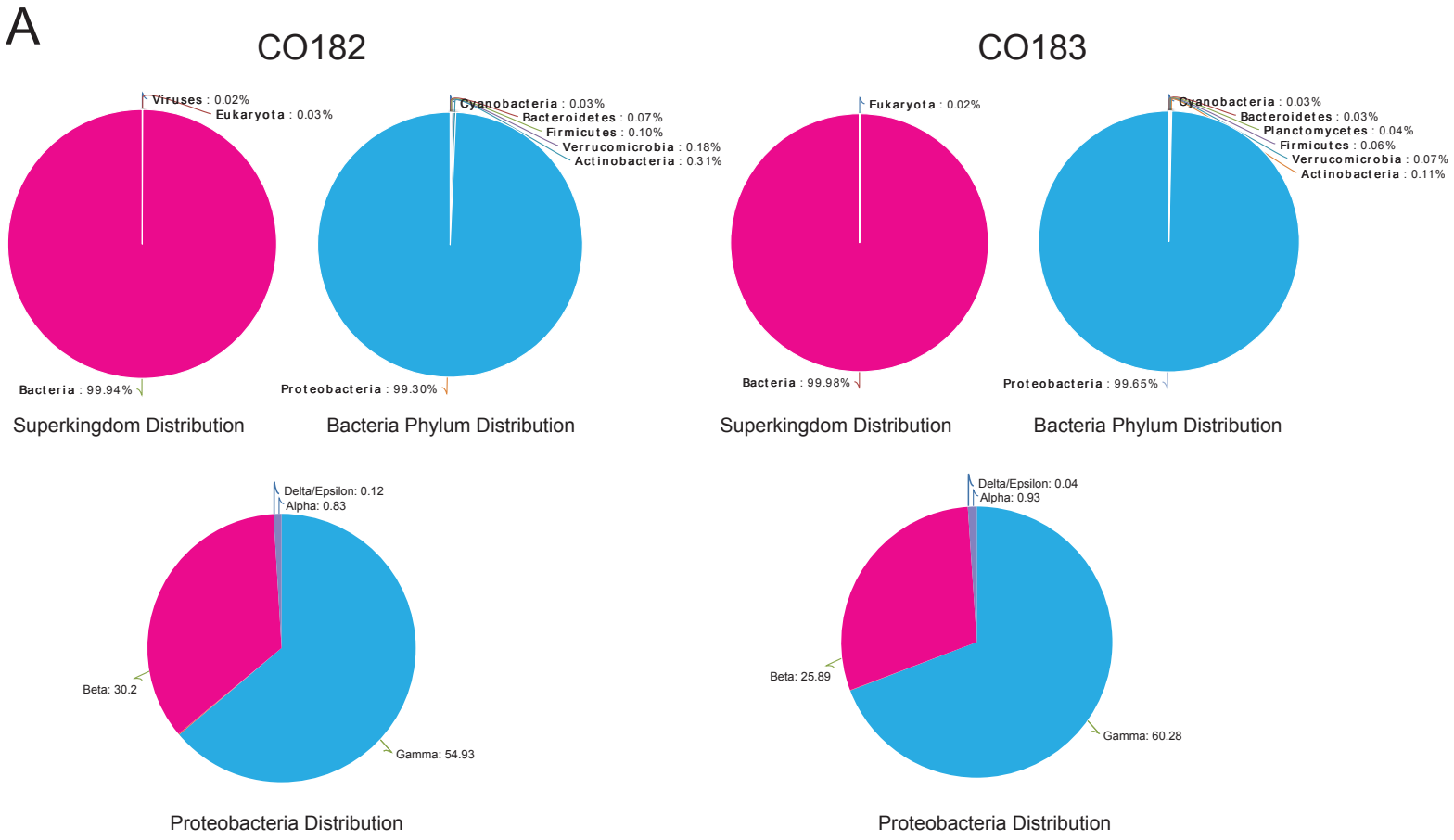
A
CO182
Viruses : 0.02%
Eukaryota : 0.03%
Bacteria : 99.94%
Superkingdom Distribution
Cyanobacteria : 0.03%
Bacteroidetes : 0.07%
Firmicutes : 0.10%
Verrucomicrobia : 0.18%
Actinobacteria : 0.31%
Proteobacteria : 99.30%
Bacteria Phylum Distribution
CO183
Eukaryota : 0.02%
Bacteria : 99.98%
Superkingdom Distribution
Cyanobacteria : 0.03%
Bacteroidetes : 0.03%
Planctomycetes : 0.04%
Firmicutes : 0.06%
Verrucomicrobia : 0.07%
Actinobacteria : 0.11%
Proteobacteria : 99.65%
Bacteria Phylum Distribution
Delta/Epsilon: 0.12
Alpha: 0.83
Beta: 30.2
Gamma: 54.93
Proteobacteria Distribution
Delta/Epsilon: 0.04
Alpha: 0.93
Beta: 25.89
Gamma: 60.28
Proteobacteria Distribution

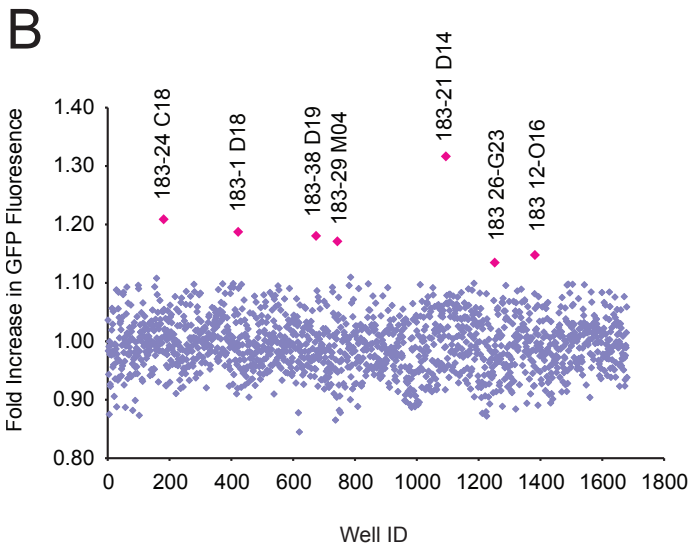
B
Fold Increase in GFP Fluoresence
1.40
1.30
1.20
1.10
1.00
0.90
0.80
0
200
400
600
800
1000
1200
1400
1600
1800
Well ID
183-24 C18
183-1 D18
183-38 D19
183-29 M04
183-21 D14
183 26-G23
183 12-O16

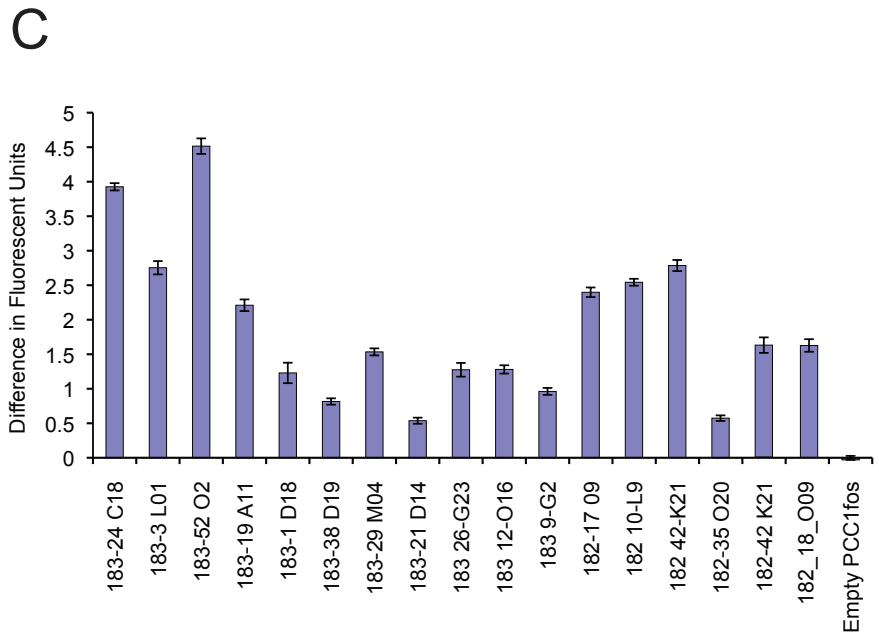
C
Difference in Fluorescent Units
5
4.5
4
3.5
3
2.5
2
1.5
1
0.5
0
183-24 C18
183-3 L01
183-52 O2
183-19 A11
183-1 D18
183-38 D19
183-29 M04
183-21 D14
183 26-G23
183 12-O16
183 9-G2
182-17 09
182 10-L9
182 42-K21
182-35 O20
182-42 K21
182_18_O09
Empty PCC1fos

Fig. S5

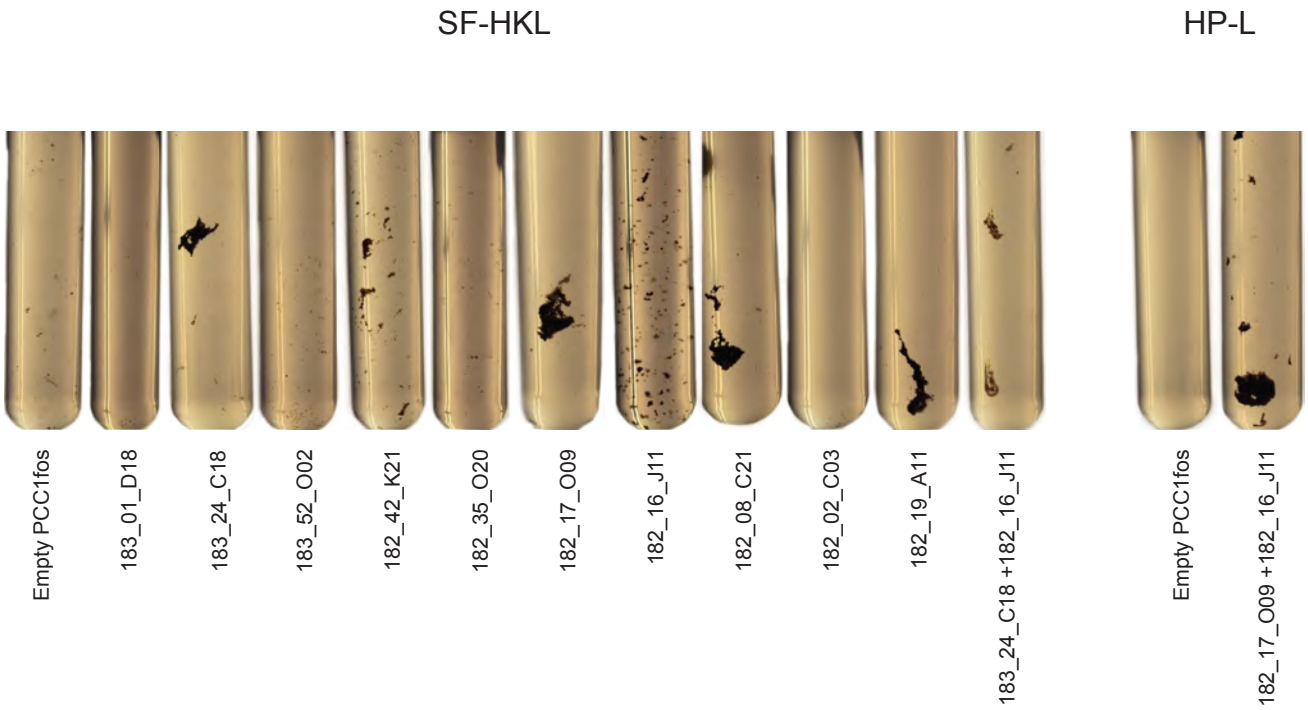
SF-HKL
HP-L
Empty PCC1fos
183_01_D18
183_24_C18
183_52_O02
182_42_K21
182_35_O20
182_17_O09
182_16_J11
182_08_C21
182_02_C03
182_19_A11
183_24_C18 +182_16_J11
Empty PCC1fos
182_17_O09 +182_16_J11

Fig. S6

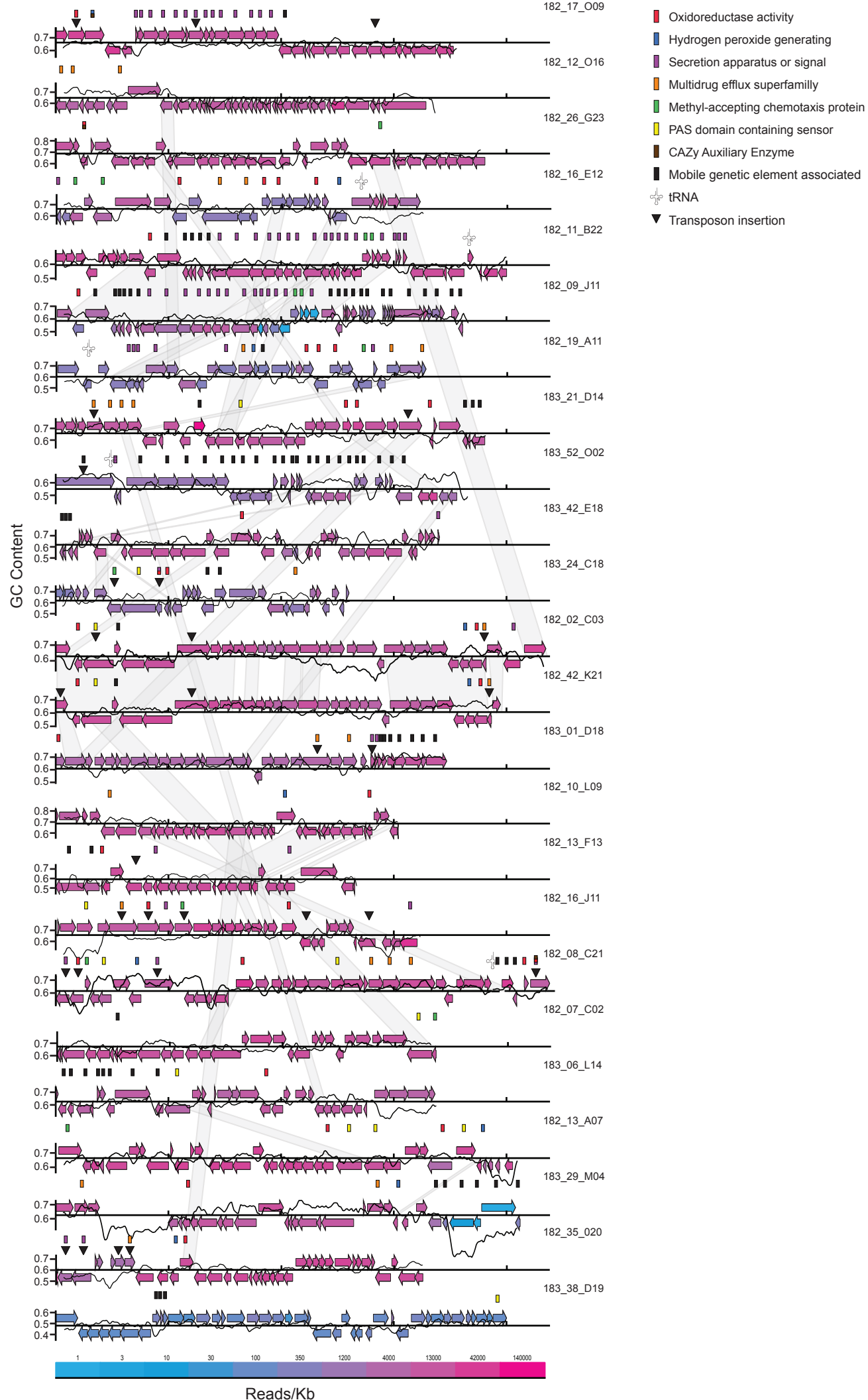
182_17_O09
182_12_O16
182_26_G23
182_16_E12
182_11_B22
182_09_J11
182_19_A11
183_21_D14
183_52_O02
183_42_E18
183_24_C18
182_02_C03
182_42_K21
183_01_D18
182_10_L09
182_13_F13
182_16_J11
182_08_C21
182_07_C02
183_06_L14
182_13_A07
183_29_M04
182_35_020
183_38_D19
GC Content
Oxidoreductase activity
Hydrogen peroxide generating
Secretion apparatus or signal
Multidrug efflux superfamilly
Methyl-accepting chemotaxis protein
PAS domain containing sensor
CAZy Auxiliary Enzyme
Mobile genetic element associated
tRNA
Transposon insertion
1
3
10
30
100
350
1200
4000
13000
42000
140000
Reads/Kb

Fig. S7

A

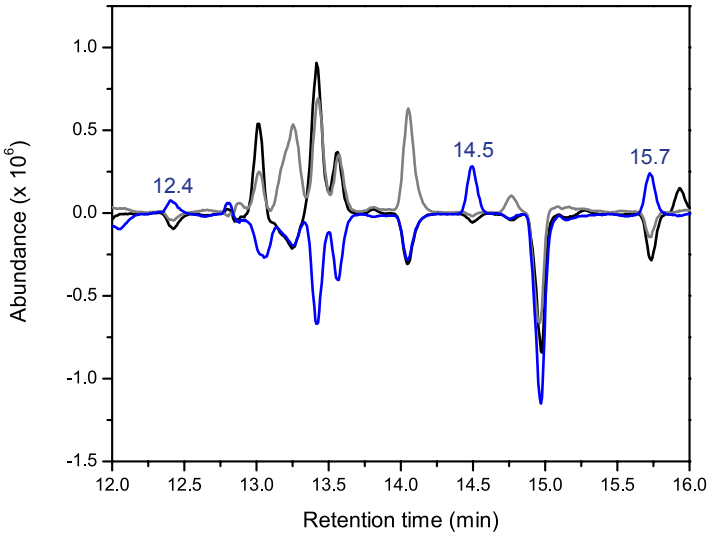

B

```
Homo sapiens (1KCW)                    3 KHYYIGIIETTAGRLYKKAPVWLGFLGPIIKAETGDKVYVHLKNLASRPYTFHSHGITYYKEHEGDDKVY 72
Botrytis aclada (3SQR)                68 REYWLSVENSTDGYTRSAMTFNGTVPGPAIIADWGDNLIIHVTNNLENGTSIHWHGIRQLGSYDGQCPIA 137
Streptomyces viridosporus T7A (3TAS)  14 KRIKLYAERLGGGQMGYGLKGKATIPGPLIELNEGDTLHIEFENTMDVPVSLHVHGLDYEISSDGRSDVE 83
Marine metagenome (4F7K)               2 APVELVAQPVNEGEPATMLGFNGGTPGPVLRARQGEVFDIRFQNQIGEGSAVHWHGLRIDNAMDGQDVVE 71
182_08_C21                            46 NDFDLFIGEIPTGAARTAMTINGSLPGPILRWREGDTVTLRVRNRLHEDTSIHWHGIILPANMDGFHGIA 115
Thermus thermophilus (2XU9)           17 LSLKLSATPTPAGQRATLLTYGGSFPGPTLRVRPRDTVRLTLENRLPEPTNLHWHGLPISPKVDDFLEIP 86

Homo sapiens (1KCW)                   73 PGEQYTYMLLATECVTRIYHSHIDKDIASGLIGPLIICKKKHIDREFVVMFSVYSVNPGLSMCAEDEVNW 142
Botrytis aclada (3SQR)               138 PGDTLTYKFQVTQYGTTWYHSHFSLQYGDGLFGPLIINGPADYDEDVVIFLQDTLMNFELTFVEGEWVVY 207
Streptomyces viridosporus T7A (3TAS)  84 PGGTRTYTWRTHVAGYWHYHDHVVGGIRNGLYGPVIVRRKVLPDRTHTIVFNDMTINPDFEATVGDRVEF 153
Marine metagenome (4F7K)              72 AGGEFEYSFRAPDAGTFWYHSHNREQVAKGLYGPLIVEEPPDVDHDLIIMIDDARALPVTPVRRGQTARI 141
182_08_C21                           116 PDGMYEYKFDVNQNGTYWYHSHSGLQEQAGVYGALVIDAKFSYDRDYVVLLSDIDMSWTGIFKPGERVRI 185
Thermus thermophilus (2XU9)           87 PGESWTYEFTVPKAGTFWYHPHLHPQLFAGLLGALVVESSLREAEEHLLVLKDVLVNRPTLVAQKQTVEW 156

Homo sapiens (1KCW)                  143 YLMGIDLHTVHFHGHSFQYKHRGVYSSDVFDIFPGTYQTLEMFPRTPGIWLLHCHVTDHIHAGMETTYT 211
Botrytis aclada (3SQR)               208 VIEDGIWHPIHLHGHDFFIVAQETDRRDVAALPGNGYLAIAFKLDNPGSWLLHCHIAWHASEGLAMQFV 276
Streptomyces viridosporus T7A (3TAS) 154 VMITEYYHTFHLHGHRWADNRTGMLIDNKICGPADGFQVIAGEGVGAGAWMYHCHVQSHSDMGMVGLFL 222
Marine metagenome (4F7K)             142 RLVNRFPHGIHLHGHHFFEVGADGNLRDTTLVDAGETRDIVCVFDNPGNWLLHCHMLGHQAAGMKTWVE 210
182_08_C21                           186 TLVNMMTHPIHLHGMWSDLEDENGNRKHTIDIPPGSKRSYRVTADALGRWAYHCHLLLHMEMGMFREVR 254
Thermus thermophilus (2XU9)          157 EVENDMDHPFHLHVHPFQVLSVGGRWKDVVNLKAGEVARLLVPLREKGRTVFHCHIVEHEDRGMMGVLE 225
```

C

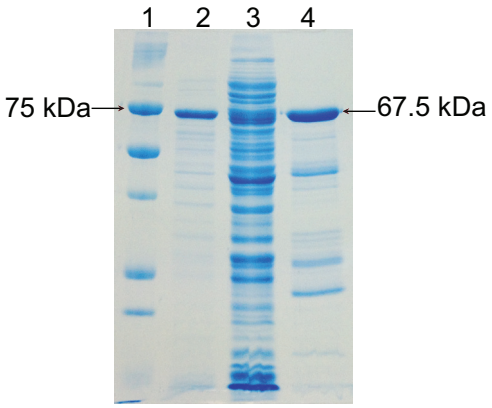

D

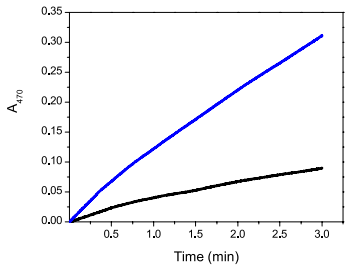

E

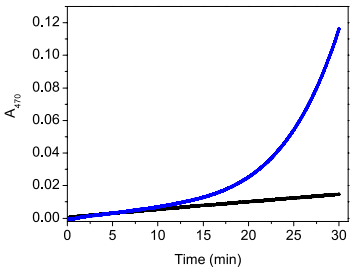

Fig. S8

A

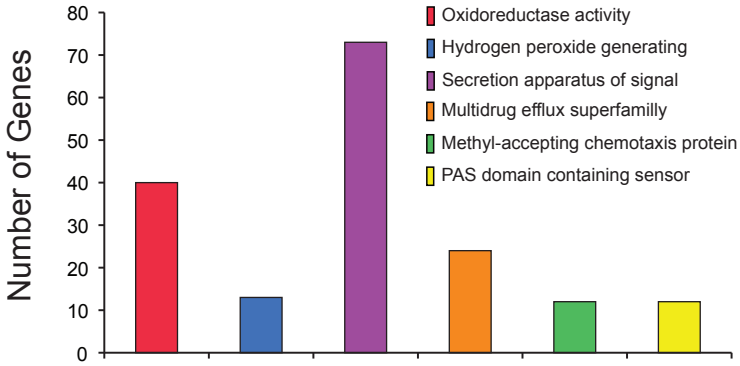
Number of Genes
0
10
20
30
40
50
60
70
80
Oxidoreductase activity
Hydrogen peroxide generating
Secretion apparatus of signal
Multidrug efflux superfamilly
Methyl-accepting chemotaxis protein
PAS domain containing sensor

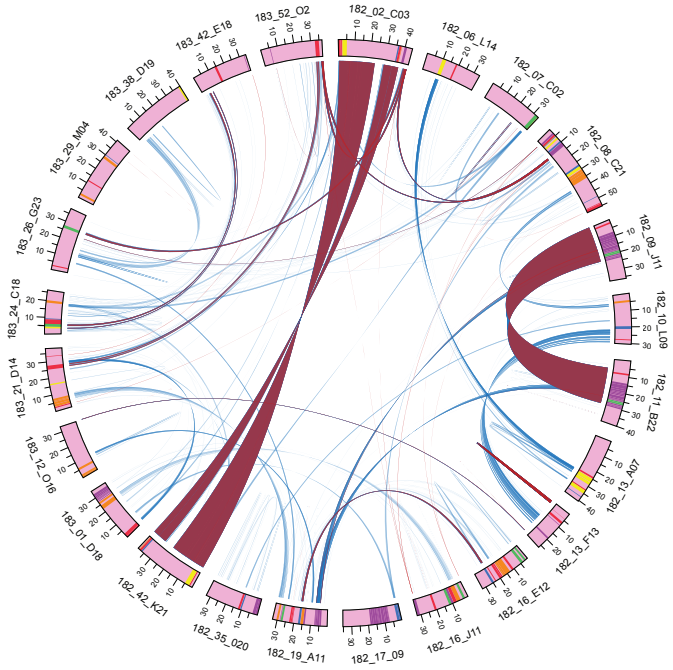
183_52_O2
182_02_C03
182_06_L14
182_07_C02
182_08_C21
182_09_J11
182_10_L09
182_11_B22
182_13_A07
182_13_F13
182_16_E12
182_16_J11
182_17_09
182_19_A11
182_35_020
182_42_K21
183_01_D18
183_12_O16
183_21_D14
183_24_C18
183_26_G23
183_29_M04
183_38_D19
183_42_E18

B

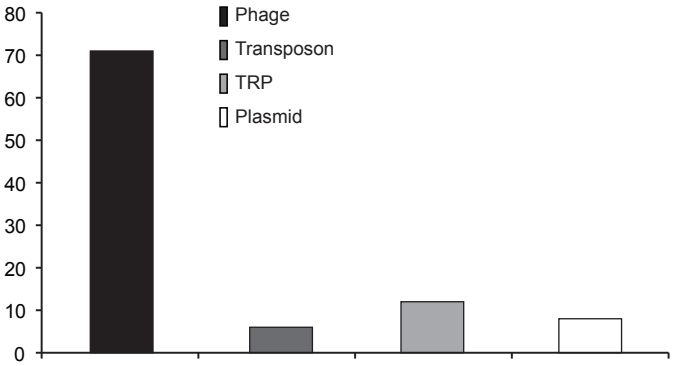
0
10
20
30
40
50
60
70
80
Phage
Transposon
TRP
Plasmid

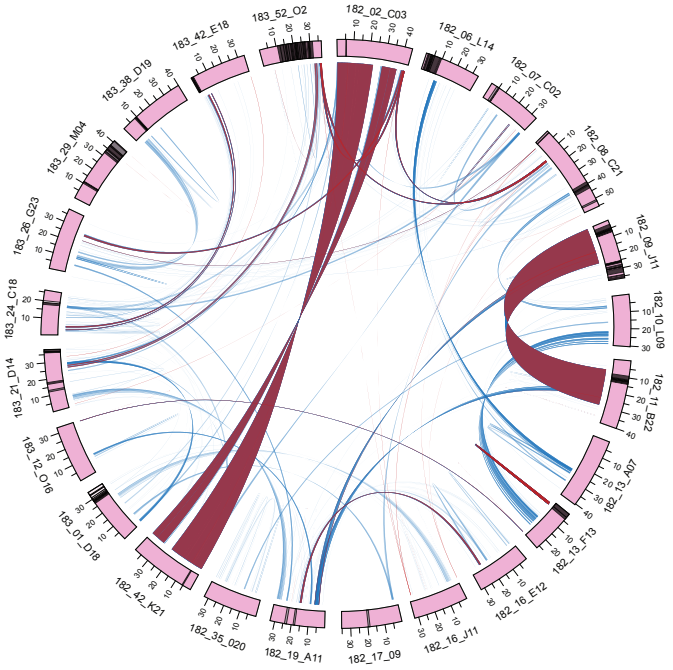
183_52_O2
182_02_C03
182_06_L14
182_07_C02
182_08_C21
182_09_J11
182_10_L09
182_11_B22
182_13_A07
182_13_F13
182_16_E12
182_16_J11
182_17_09
182_19_A11
182_35_020
182_42_K21
183_01_D18
183_12_O16
183_21_D14
183_24_C18
183_26_G23
183_29_M04
183_38_D19
183_42_E18

Fig. S9

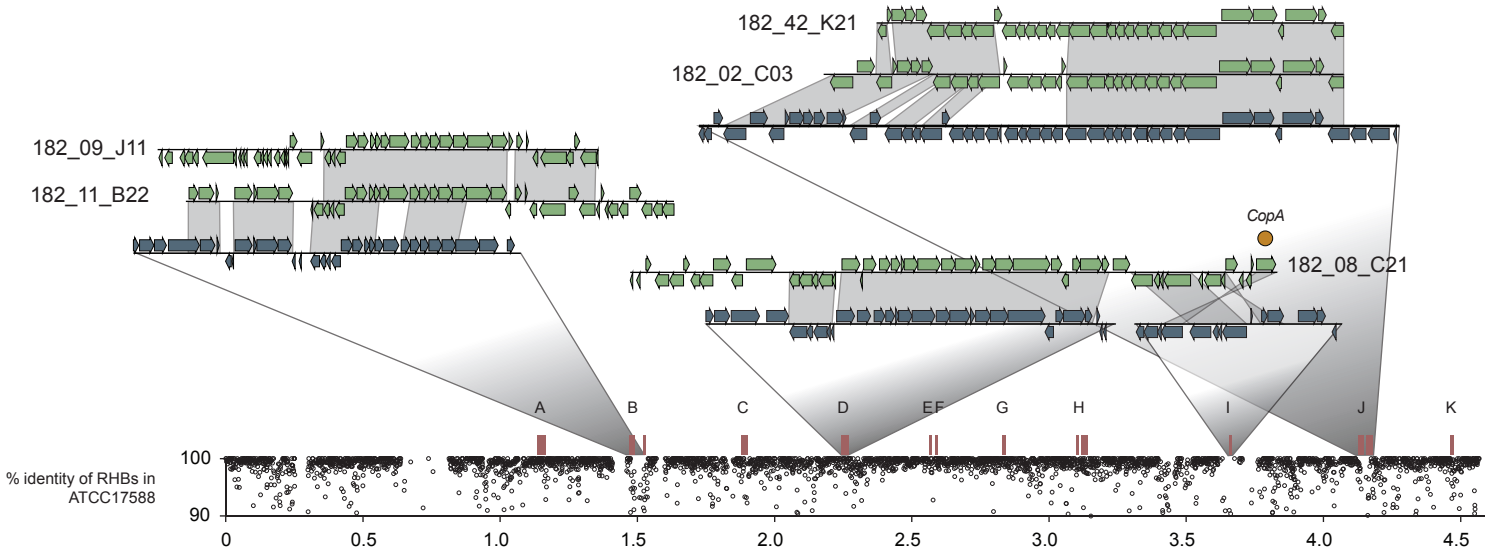

	Fosmid ID
A	182_35_020
B	182_09_J11, 182_11_B22
C	182_17_09
D	182_08_C21
E	182_06_L14
F	182_16_E12
G	182_13_F13
H	182_13_A07
I	182_08_C21
J	182_02_C03, 182_42_K21
K	182_16_J11

Fig. S10

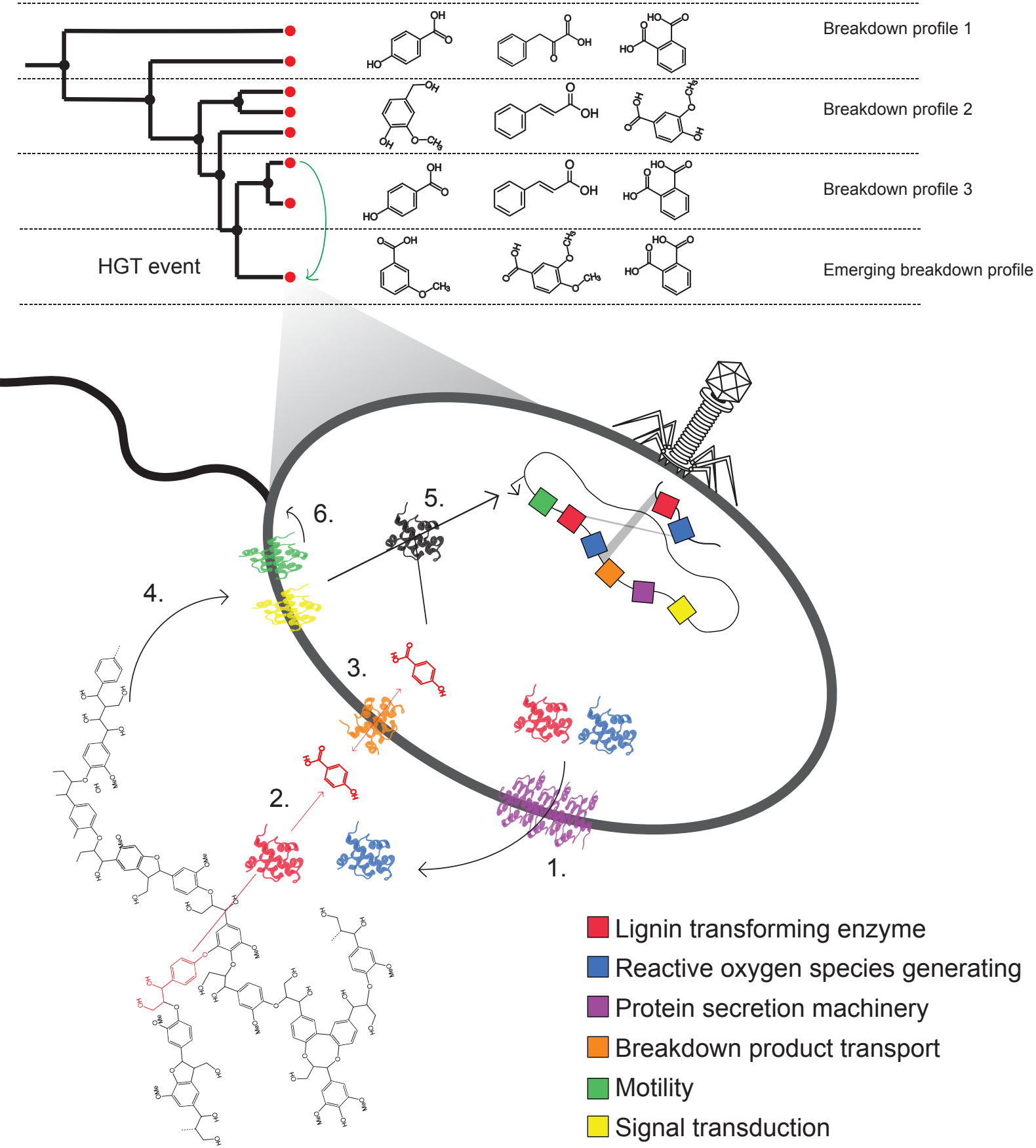
Breakdown profile 1
Breakdown profile 2
Breakdown profile 3
Emerging breakdown profile
HGT event
1.
2.
3.
4.
5.
6.
Lignin transforming enzyme
Reactive oxygen species generating
Protein secretion machinery
Breakdown product transport
Motility
Signal transduction

Fig. S11